Electr Eng (2015) 97:195–204
DOI 10.1007/s00202-014-0326-x

ORIGINAL PAPER

Generalized predictive control robust for position control of induction motor using field-oriented control

Wellington A. Silva · Antonio B. S. Junior · Bismark C. Torrico · Dalton A. Honório · Tobias R. Fernandes Neto · Laurinda L. N. dos Reis · Luiz H. S. C. Barreto

Received: 25 February 2014 / Accepted: 26 December 2014 / Published online: 9 January 2015

Abstract This paper presents the study and implementation of a different field-oriented control strategy using a generalized predictive control (GPC) technique applied to the mechanic position loop aiming to obtain a system that acts in the fractional horsepower motor driver running at near zero frequency. The position and speed loops were identified to verify the system behavior and, from the model found design the GPC controller. Simulation and experimental results are shown and discussed to demonstrate the merit of the proposed approach and the performance and robustness of the algorithms have been evaluated.

Keywords Field-oriented control · Predictive control · Position control · Robustness

1 Introduction

Induction machines (IM) are widely used in industry due to simplicity, lower cost, reduced need for maintenance, and also greater robustness if compared to other types of electrical machines. The main difficulty of using the IM for position control is the mathematical modeling of the controller design. Typically, position control of the motor shaft is performed by employing DC motors and servomotors. In the last two decades, advances have occurred in the study of principles that govern field oriented control (FOC) applied to alternating current (AC) machines. Therefore, the control of induction machines can achieve performances similar to those of DC motors. The machine currents and voltages using FOC allow the direct control of the spatial orientation of electromagnetic fields, resulting in the use of the term "field-oriented" for this type of controller. In this type of control, a direct analogy can be established with the control of a DC motor with separate excitation [1].

There are several techniques for speed control applied to IM drives, such as the use of predictive strategies. The predictive model was employed in [2] to control both the speed and rotor flux. Additionally, in [3] uses a strategy predictive applied to the direct torque control (DTC) to decrease flux and torque ripple. Technical adaptations are widely used in [4], which uses the strategy named model reference adaptive control (MRAC) to control speed in the IM. Besides there are robust techniques of DTC to speed sensorless adjust using a predictive controller in a PI structure [5].

Recently, structures mixing various types of controllers known as hybrid controllers have been proposed by several researchers to achieve the best performance for each strategy. In [6] was used a hybrid PID controller, which has the advantage of being easily tuned by a fuzzy controller with the aim of improving the system robustness. In [7] was proposed a new robust MRAC using a hybrid strategy, where fuzzy logic is then used to achieve the hybridization between sliding mode control (SMC) and a PI controller for flux and speed control in the IM.

To control the shaft position in IMs considering that speed is almost zero, a proper strategy is necessary, while studies regarding this subject are rarely found in literature. A sensorless control for the IM using harmonic pulse width modulation (PWM) was proposed in [8].

The strategy named internal model control (IMC) to achieve zero speed was used in [9], while in other work was used variable structure control (VSC) with adaptive gain in the speed loop for the positioning of IM [10]. The fuzzy logic to control the IM was employed in [11]. The SMC strategy was utilized in position loop in [12]. Previous works have

W. A. Silva · A. B. S. Junior (✉) · B. C. Torrico · D. A. Honório · T. R. F. Neto · L. L. N. dos Reis · L. H. S. C. Barreto
Fortaleza, Brazil
e-mail: barbosa@dee.ufc.br

also presented a comparison between SMC and the use of FOC applied to the speed control for the IM operating at low speeds, presented in [13].

Therefore, this paper proposes the design of the controller that acts on the position loop to achieve the positioning of the IM shaft. Substituting loop speed control by the position control strategy using GPC with RST polynomial structure of control [14], i.e., instead of having two controllers, one for position and one for speed, as shown in classic strategy, there is only a block position controller.

The technology contribution of this study lies in the possible applications to robotics. When induction motors (IMs) are used, inexpensive, rugged, and easy to maintain units can be used in the joint degrees of freedom of the robot arm, for example.

The main scientific contribution consists in the study GPC applied to position control of IM. The use of the aforementioned control techniques GPC is justified by simplicity and ease of implementation in an embedded system. For instance, a DSC (digital signal controller) is used in the proposed approach.

Finally, this work presents simulations tests and experimental results to demonstrate the main features of the developed system, thus validating the employed methodology. The paper is organized as follows. Sections 2 and 3 describes the induction motor modeling and the controllers design, respectively. After, in Sect. 4 a design scheme of robust GPC controller is proposed. The Sect. 5 presents the discussion of both simulation and experimental results, respectively. Finally, the proper conclusions are given in Sect. 6.

2 Dynamic modelling of the indirect field-oriented control of an induction machine

The block diagram of the indirect field-oriented induction motor drive is shown in Fig. 1. The state equations of the induction motor in the synchronously rotating reference frame can be described by [1] as:

$$\frac{\mathrm{d}}{\mathrm{d}t}[A] = [B][C] + \frac{1}{\sigma L_\mathrm{s}}[D], \tag{1}$$

where

$$[A] = \begin{bmatrix} i_{\mathrm{ds}} \\ i_{\mathrm{qs}} \\ \lambda_{\mathrm{dr}} \\ \lambda_{\mathrm{qr}} \end{bmatrix}; \quad [C] = \begin{bmatrix} i_{\mathrm{ds}} \\ i_{\mathrm{qs}} \\ \lambda_{\mathrm{dr}} \\ \lambda_{\mathrm{qr}} \end{bmatrix}; \quad [D] = \begin{bmatrix} v_{\mathrm{ds}} \\ v_{\mathrm{qs}} \\ 0 \\ 0 \end{bmatrix};$$

$$[B] = \begin{bmatrix} -\frac{R_\mathrm{s}}{\sigma L_\mathrm{s}} - \frac{R_\mathrm{r}(1-\sigma)}{\sigma L_\mathrm{r}} & \omega_\mathrm{e} & \frac{L_\mathrm{m} R_\mathrm{r}}{\sigma L_\mathrm{s} {L_\mathrm{r}}^2} & \frac{P\omega_\mathrm{r} L_\mathrm{m}}{2\sigma L_\mathrm{s} {L_\mathrm{r}}^2} \\ \omega_\mathrm{e} & -\frac{R_\mathrm{s}}{\sigma L_\mathrm{s}} - \frac{R_\mathrm{r}(1-\sigma)}{\sigma L_\mathrm{r}} & \frac{-P\omega_\mathrm{r} L_\mathrm{m}}{2\sigma L_\mathrm{s} {L_\mathrm{r}}^2} & \frac{L_\mathrm{m} R_\mathrm{r}}{\sigma L_\mathrm{s} {L_\mathrm{r}}^2} \\ \frac{L_\mathrm{m} R_\mathrm{r}}{L_\mathrm{r}} & 0 & -\frac{R_\mathrm{r}}{L_\mathrm{r}} & \omega_\mathrm{e} - \frac{P}{2}\omega_\mathrm{r} \\ 0 & \frac{L_\mathrm{m} R_\mathrm{r}}{L_\mathrm{r}} & -\left(\omega_\mathrm{e} - \frac{P}{2}\omega_\mathrm{r}\right) & -\frac{R_\mathrm{r}}{L_\mathrm{r}} \end{bmatrix}; \tag{2}$$

The torque is given by:

$$T_\mathrm{e} = \frac{3P}{4}\frac{L_\mathrm{m}}{L_\mathrm{r}}(i_{\mathrm{qs}}\lambda_{\mathrm{dr}} - i_{\mathrm{ds}}\lambda_{\mathrm{qr}}), \tag{3}$$

While expressions (4), (5), (6) give the following parameters:

$$\sigma = 1 - \frac{{L_\mathrm{m}}^2}{L_\mathrm{s} L_\mathrm{r}}, \tag{4}$$

$$\lambda_{\mathrm{qr}} = L_\mathrm{m} i_{\mathrm{qs}} + L_\mathrm{r} i_{\mathrm{dr}}, \tag{5}$$

$$\lambda_{\mathrm{dr}} = L_\mathrm{m} i_{\mathrm{ds}} + L_\mathrm{r} i_{\mathrm{qr}}, \tag{6}$$

where,

T_e = Electromagnetic torque (Nm)
T_L = Load torque (Nm)
R_s = Stator resistance (Ω)
L_s = Stator magnetizing inductance (H)
L'_s = Stator transient inductance (H)
R_r = Rotor resistance (Ω)
L_r = Rotor magnetizing inductance (H)
L_m = Magnetizing inductance (H)
P = Number of poles, adimensional
ω_e = Electrical angular speed (rad/s)
ω_r = Rotor angular speed (rad/s)
ω_sl = Slip angular speed (rad/s)
v_{ds} = d-axis stator voltage (V)
v_{qs} = q-axis stator voltage (V)
i_{ds} = d-axis stator current (A)
i_{qs} = q-axis stator current (A)
i^*_{ds} = d-axis stator current command (A)
i^*_{qs} = q-axis stator current command (A)
λ_{qr} = Rotor flux align with the q-axis (Wb)
λ_{dr} = Rotor flux align with the d-axis (Wb)
σ = Magnetic coupling constant, adimensional

Accordingly, the flux linkage and its derivative in the q-axis are set to zero as:

$$\lambda_{\mathrm{qr}} = 0 \quad \text{and} \quad \frac{\mathrm{d}\lambda_{\mathrm{qr}}}{\mathrm{d}t} = 0, \tag{7}$$

In an ideal field-orientated induction motor, decoupling between d and q-axis can be achieved, while the total rotor flux linkage is forced to align with the d-axis. Then resulting in (8) and (9)

$$v_{\mathrm{qs}} = (R_\mathrm{s} + L'_\mathrm{s}) i_{\mathrm{qs}} + \omega_\mathrm{e} L_\mathrm{s} i_{\mathrm{ds}}, \tag{8}$$

$$v_{\mathrm{ds}} = r_\mathrm{s} i_{\mathrm{ds}} - \omega_\mathrm{e} L'_\mathrm{s} i_{\mathrm{qs}}, \tag{9}$$

where,

$$L'_\mathrm{s} = L_\mathrm{s} - \frac{L_\mathrm{m}^2}{L_\mathrm{r}}, \tag{10}$$

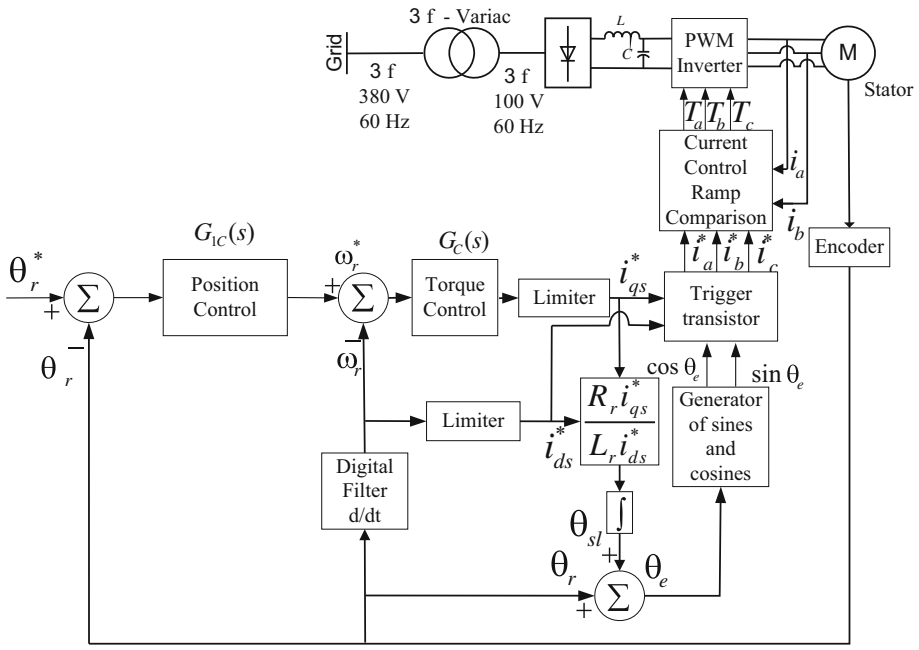

Fig. 1 Block diagram representing field-oriented induction motor drive

The rotor flux linkage can be found from the third row in (1) and by using (4) as:

$$\lambda_{\mathrm{dr}} = \frac{L_{\mathrm{m}} i_{\mathrm{ds}}}{1 + s\frac{L_{\mathrm{r}}}{R_{\mathrm{r}}}}, \tag{11}$$

According to (11), since the electrical time constant $(L_{\mathrm{r}}/R_{\mathrm{r}})$ is much smaller (near to zero) than the mechanical one, it can be neglected. As a result, the current i_{ds} is constant $(i_{\mathrm{ds}} = i_{\mathrm{ds}}^*)$ and the desired rotor flux will be constant either. Thus, the Eq. (11) becomes:

$$\lambda_{\mathrm{dr}} = L_{\mathrm{m}} i_{\mathrm{ds}}^*, \tag{12}$$

From (4) and (6), expression (3) is simplified to:

$$T_{\mathrm{e}} = \frac{3P}{4}\frac{L_{\mathrm{m}}^2}{L_{\mathrm{r}}} i_{\mathrm{qs}}^* \tag{13}$$

where i_{qs} denotes the torque current command generated from the torque controller $G_{\mathrm{c}}(s)$. When using indirect field orientation, the slip angular speed is necessary to calculate the unit vector for coordinate translation. By employing the fourth row of (1) and also (4), the slip angular frequency ω_{sl} can be estimated as:

$$\omega_{\mathrm{sl}} = \frac{L_{\mathrm{m}} R_{\mathrm{r}} i_{\mathrm{qs}}^*}{L_{\mathrm{r}} \lambda_{\mathrm{dr}}} = \frac{R_{\mathrm{r}} i_{\mathrm{qs}}^*}{L_{\mathrm{r}} i_{\mathrm{ds}}^*} \tag{14}$$

The generated torque T_{e}, rotor speed ω_{r}, and rotor angular position θ_{r} are related by:

$$\omega_{\mathrm{r}} = s\theta_{\mathrm{r}} = \frac{1/J}{s + B/J}[T_{\mathrm{e}}(s) - T_{\mathrm{L}}(s)] \tag{15}$$

where B is the viscous damping coefficient, J is the inertia constant, and T_{L} is the load torque applied to the shaft.

3 GPC approach to model predictive control

The predictive control strategy requires a system model under study to compute the prediction inside the control horizons to be used. So it is needed a preliminary study to find the model that best suit the system. Thereby, the predictive controller can be implemented. This section is subdivided into two subsections, one relating to the system modeling and another to the predictive control used.

3.1 System modeling

In the identification of the model system there are various types of methodologies. For this process represented in Fig. 1, the structure of the FOC scheme has been changed and presented in Fig. 2. Then was performed some steps in torque reference system being analyzed the output of rotor speed. This behavior can be observed in Fig. 3. This data was used to identify the model, where half of the data was used for the identification process and the other half used for validation.

The process dynamics can be represented using the Controlled Auto-Regressive and Integrated Moving Average (CARIMA) model [14,15]:

$$A(q^{-1})y(t) = B(q^{-1})u(t) + \frac{C(q^{-1})}{\Delta}e(t), \tag{16}$$

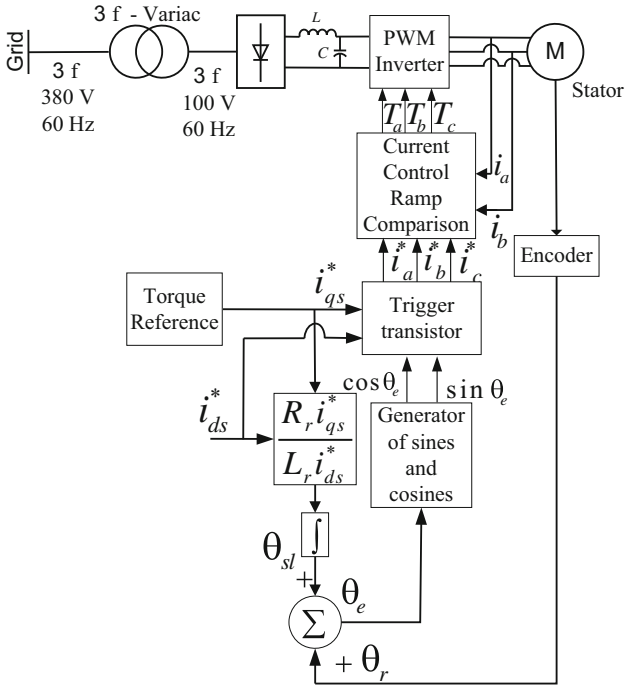

Fig. 2 Structure used for identification

where $e(t)$ is uncorrelated (white) noise with zero mean value, $A(q^{-1})$, $B(q^{-1})$ and $C(q^{-1})$ are polynomials in the backward shift operator q^{-1} in the form and $\Delta = 1 - q{-}1$:

$$A(q^{-1}) = 1 + a_1 q^{-1} + a_2 q^{-2} + \cdots + a_{\mathrm{na}} q^{-\mathrm{na}},$$
$$B(q^{-1}) = b_0 + b_1 q^{-1} + b_2 q^{-2} + \cdots + b_{\mathrm{nb}} q^{-\mathrm{nb}},$$
$$C(q^{-1}) = 1 + c_1 q^{-1} + c_2 q^{-2} + \cdots + c_{\mathrm{nc}} q^{-\mathrm{nc}}.$$

From the data obtained in Fig. 3, the least squares method was used [14], and considering Eq. (16) with $n_a = 2$ and $n_b = 1$, the following discrete transfer function relating rotor speed output and reference torque is given by:

$$G(q^{-1}) = \frac{B(q^{-1})}{A(q^{-1})} = \frac{0.00691 + 0.005857q^{-1}}{1 - 0.9775q^{-1} - 0.002285q^{-2}} \tag{17}$$

The polynomial $C(q^{-1})$ corresponds the model noise dynamics is modeled by a filter in following section. As the proposed controller is in the loop position, so just add an integrator in the system model.

3.2 Generalized predictive control

The GPC algorithm consists in applying a control sequence that minimizes a multistage cost function of the form [15]:

$$J = \sum_{j=N_1}^{N_2} [y(t+j|t) - \omega(t+j)]^2 + \sum_{j=0}^{Nu-1} \lambda[\Delta u(t+j|1)]^2, \tag{18}$$

where N_1 and N_2 are the minimum and maximum costing horizons, respectively, N_{u} is the control horizon, λ is the control weight, $\omega(t+j)$ is a future setpoint or reference sequence, $\Delta u(t)$ is the incremental control action and $y(t+j|t)$ is the optimum j-step ahead prediction of the system output $y(t)$ on data up to time t.

The solution of this optimization problem is a crucial step in MPC (model-based control) algorithms. The numerical complexity depends on the characteristics of the models in terms of linearity, constraints, number of manipulated and controlled variables, etc. For linear models without constraints, the MPC optimization can be performed analytically [16].

The future outputs can be computed using filtering techniques or Diophantine equations [16] while this work uses the second approach. To compute the future outputs $y(t+j)$ for $j = N1, \ldots, N2$, the following Diophantine equation must be solved:

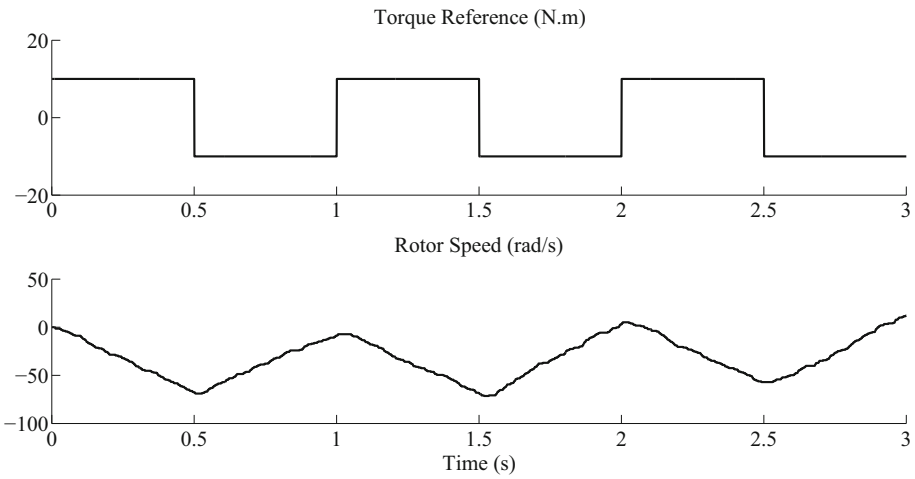

Fig. 3 Input and output for system identification

$$C(q^{-1}) = E_j(q^{-1})\Delta A(q^{-1}) + q^{-1}F_j(q^{-1}), \quad (19)$$

where $E_j(q^{-1})$ and $F_j(q^{-1})$ are uniquely defined polynomials with degrees $j-1$ and n_a, respectively.

Using Eqs. (16) and (19) the future process output can be described by:

$$y(t+j) = \frac{F_j(q^{-1})}{C(q^{-1})}y(t) + \frac{E_j(q^{-1})B(q^{-1})}{C(q^{-1})}\Delta u(t+j-1) + E_j(q^{-1})e(t+j). \quad (20)$$

As the degree of $E_j(q^{-1})$ is $j-1$, then all the noise terms are in the future, and therefore the optimal prediction can be obtained replacing $e(t+j)$ for its expected value (zero) as:

$$y(t+j|t) = \frac{F_j(q^{-1})}{C(q^{-1})}y(t) + \frac{E_j(q^{-1})B(q^{-1})}{C(q^{-1})}\Delta u(t+j-1|t). \quad (21)$$

From Eq. (21), the past control inputs can be separated solving a new Diophantine equation:

$$E_j(q^{-1})B_j(q^{-1}) = H_j(q^{-1})C(q^{-1}) + q^{-j}I_j(q^{-1}), \quad (22)$$

where $H_j(q^{-1})$ has degree $j-1$ and $I_j(q^{-1})$ has degree $n_i = \max(n_a, n_b - j - 1)$. Using Eqs. (21) and (22) the prediction output can be written as:

$$y(t+j|t) = \frac{F_j(q^{-1})}{C(q^{-1})}y(t) + \frac{I_j(q^{-1})}{C(q^{-1})}\Delta u(t-1) + H_j(q^{-1})\Delta u(t+j-1|t), \quad (23)$$

which can be expressed in a vector form as:

$$y = F_j(q^{-1})\frac{y(t)}{C(q^{-1})} + I(q^{-1})\frac{\Delta u(t-1)}{C(q^{-1})} + G\Delta u, \quad (24)$$

where

$$\mathbf{y} = [y(t+N_1|t)\, y(t+N_1+1|t) \cdots y(t+N_2|t)]^T,$$
$$\Delta\mathbf{u} = [\Delta u(t|t)\, u(t+1|t) \cdots u(t+N_u-1|t)]^T,$$

and G is a $N \times N_u$ constant matrix based on the coefficients of $H_j(q^{-1})$, while $F(q^{-1})$ and $I(q^{-1})$ are polynomial vectors.

From controller implementation standpoint, an analytical solution with low computational cost is important. Thus, this work is concerned with the investigation of a especial case where $N_u = 1$, $N_1 = 1$, $N_2 = N$ and $\lambda = 0$, which represents the best tradeoff between the computational cost and close loop performance [17], then the optimal input is [18]:

$$\Delta u(t) = (G^T G)^{-1}G^T(w - f) = k(w - f), \quad (25)$$

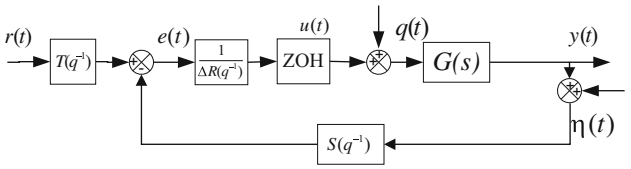

Fig. 4 Classical RST structure

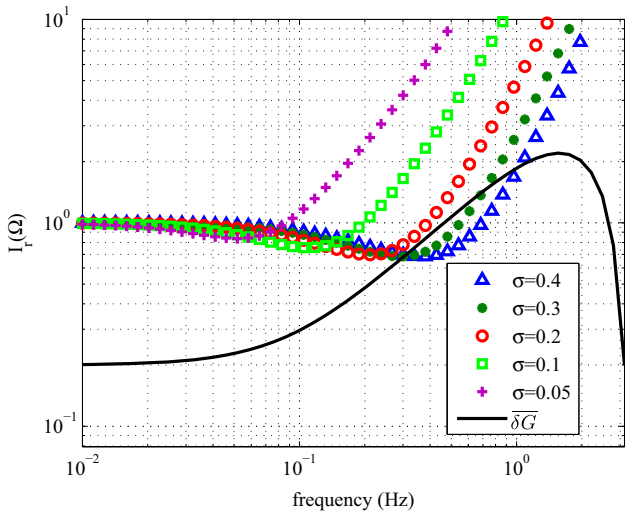

Fig. 5 Robustness index

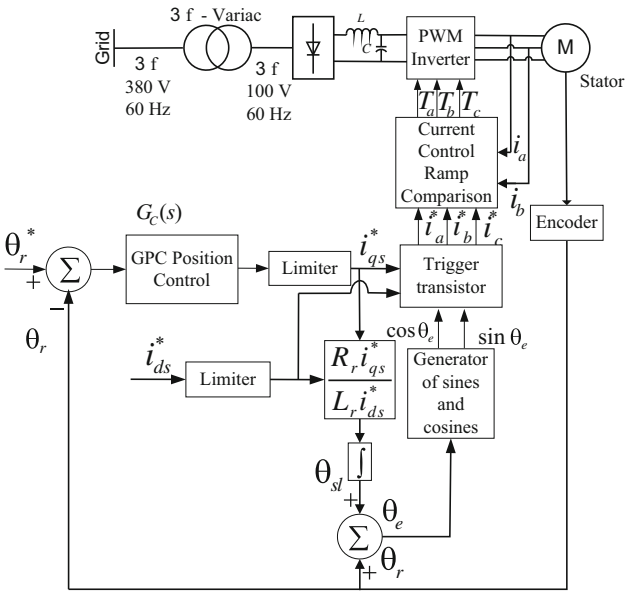

Fig. 6 Control structure proposed position using GPC

where $\mathbf{k}$ is a constant vector with dimension $1 \times N$, w is a vector which contains the future reference and free response given by:

$$f = F(q^{-1})\frac{y(t)}{C(q^{-1})} + I(q^{-1})\frac{\Delta u(t-1)}{C(q^{-1})}, \quad (26)$$

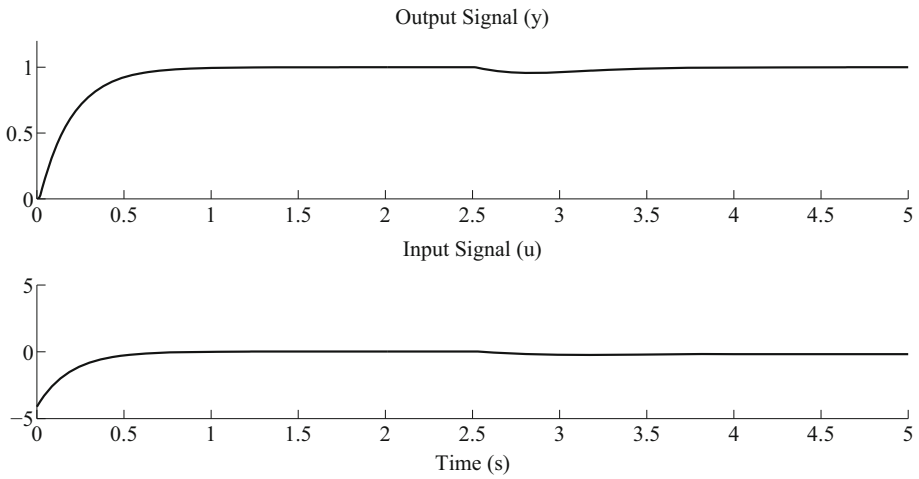

Fig. 7 Simulation results for the system model using the GPC control strategy

Since $N_u = 1$, it is important to notice that the constrained controller is equivalent to clipping, a case valid only for monovariable systems [19]. The term clipping assumes that the predictive controller does not take into account constraints while computing the optimal input, but only afterwards, performing hard limitations if constraints are violated.

Through some manipulations, Eq. (25) can be written in the RST form:

$$u(t) = \frac{1}{\Delta R(q^{-1})}(T(q^{-1})r(t) - S(q^{-1})y(t)), \tag{27}$$

where $r(t) = w(t + j)$ is the setpoint, $T(q^{-1}) = C(q^{-1})\sum_{i=1}^{N} k(i)$, $S(q^{-1}) = \sum_{i=1}^{N} k(i)F_i(q^{-1})$, $R(q^{-1}) = C(q^{-1}) + q^{-1}\sum_{i=1}^{N} k(i)I_i(q^{-1})$. The RST structure is important from control analysis standpoint because it can be derived properties such as stability and robustness.

Table 1 Motor parameters

Parameters	Value
Rated power	0.25 HP
Rated speed	1,725 rpm
Rated voltage	220 V
Rated current	1.26 A
Number of poles	4
Rotor resistance (referred to the stator)	87.44 Ω
Stator resistance	35.58 Ω
Rotor inductance (referred to the stator)	0.16 H
Stator inductance	0.16 H
Mutual inductance	0.884 H
Inertia moment	5×10^{-4} kg m^2
Viscous friction coefficient	5.65×10^{-3} kg m^2/s

4 Robust GPC-based control (GPCBC) applied to IM position loop

From model Eq. (16) the polynomial $C(q^{-1})$ is a monic that can be treated as a filter [16]. The selection of $C(q^{-1})$ is not a trivial matter, some guidelines for open-loop stable processes and some case studies can be found in literature [19]. In this study, the process is of second-order, then the $C(q^{-1})$ polynomial, it is enough to use a filter with degree $n_c = 2$ to attenuate the noise, considering that it is properly tuned [16]. Thus, the proposed filter is given by:

$$C(q^{-1}) = 1 + c_1 q^{-1} + c_2 q^{-2}, \tag{28}$$

where c_1 and c_2 are constants which must be tuned considering noise attenuation, disturbance rejection, and robustness.

Considering Eqs. (16) and (28), the control input $u(t)$ in Eq. (27) can be calculated explicitly by performing some mathematical manipulation. Thus, the control polynomials R, S, and T are given by:

$$T(q^{-1}) = t_0 + t_1 q^{-1} + t_2 q^{-2}, \tag{29}$$

$$R(q^{-1}) = 1 + r_1 q^{-1} + r_2 q^{-2}, \tag{30}$$

$$S(q^{-1}) = s_0 + s_1 q^{-1} + s_2 q^{-2}, \tag{31}$$

$$\alpha = 1 - \frac{1 + 2 + 3 + \cdots + N}{1 + 2^2 + 3^2 + \cdots + N^2}. \tag{32}$$

It is important to notice that polynomials R, S and T contain parameter a, which on the other hand depends on N. From Eq. (32), it can be seen that a varies from 0 to 1 when the prediction horizon N varies from 1 to inf. Therefore, the direct use of alpha is proposed as a tuning parameter, assuming an adjustable value between 0 and 1. It makes the tuning process more precise than the use of discrete values of the N.

The block diagram of the proposed robust GPC-based control (GPCBC) can be posed in the classical RST structure as illustrated in Fig. 4. To understand the nominal behavior, the transfer functions relating the reference with the output, the input disturbance with the output, the noise with the control

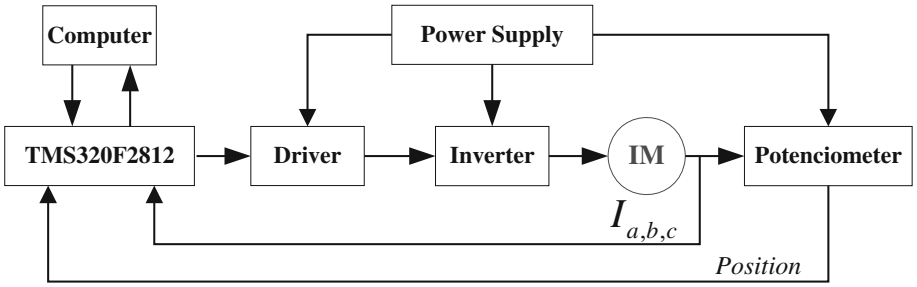

Fig. 8 Schematics of the system

input and the noise with the output are calculated as follows:

$$H_{\mathrm{yr}}(z) = \mathrm{Z}\left\{\frac{y(t)}{r(t)}\right\} = \frac{T(z)G(z)}{\Delta R(z) + S(z)G(z)}, \tag{33}$$

$$H_{\mathrm{yq}}(z) = \mathrm{Z}\left\{\frac{y(t)}{q(t)}\right\} = \frac{\Delta R(z)G(z)}{\Delta R(z) + S(z)G(z)}, \tag{34}$$

$$H_{\mathrm{un}}(z) = \mathrm{Z}\left\{\frac{u(t)}{n(t)}\right\} = \frac{-S(z)}{\Delta R(z) + S(z)G(z)}, \tag{35}$$

$$H_{\mathrm{yn}}(z) = \mathrm{Z}\left\{\frac{y(t)}{n(t)}\right\} = \frac{-S(z)G(z)}{\Delta R(z) + S(z)G(z)}, \tag{36}$$

where $Z\{.\}$ denotes z-transform, $q(t)$ is an input disturbance, and $n(t)$ is a measurement noise signal at a given discrete instants t.

Equation (33) shows that $H_{\mathrm{yr}}(z)$ is a first order transfer function which depends just on a. Therefore, faster or slower setpoint responses can be achieved by decreasing or increasing a, respectively. On the other hand, $C(z)$ can be used to change disturbance rejection response (Eq. (34)) and as a measurement noise filter to attenuate noise effect in both control and output signals [(Eqs. (35), (36), respectively]. Assuming that $C(z)$ has roots with the same real part, in manner that Eq. (28) can be rewritten as:

$$C(q^{-1}) = (1 - \mathrm{e}^{-\sigma + i\beta}q^{-1})(1 - \mathrm{e}^{-\sigma - i\beta}q^{-1}), \tag{37}$$

where σ and β are tuning parameters, and i is the imaginary operator.

The ratio β/σ imposes certain characteristics to the filter $C(z)$, and therefore, a set of filters with different ratios β/σ. In [20] is shown that the optimal second order filter has a damping $\xi = 1/\sqrt{2}$ to attenuate the noisy sensibility which implicates in $\beta = \sigma \tan(\pi/4) = \sigma$. Therefore, the filter has only one tuning parameter to disturbance rejection, noisy attenuation and robustness.

The modeling errors can be represented by $G(z) = G_{\mathrm{n}}(z)(1 + \delta G(z))$, where G_{n} is the nominal model. Considering an upper limit to the norm of $\delta G(\mathrm{e}^{\mathrm{j}\mathrm{O}})$ given by $\overline{\delta G}(\Omega)$ in the interval $0 = \Omega < p$.

The closed loop robust stability is reached if [21]:

$$\overline{\delta G}(\Omega) \leq I_{\mathrm{r}}(\Omega) = \frac{|\Delta R(z) + S(z)G(z)|}{|S(z)G(z)|}, \tag{38}$$

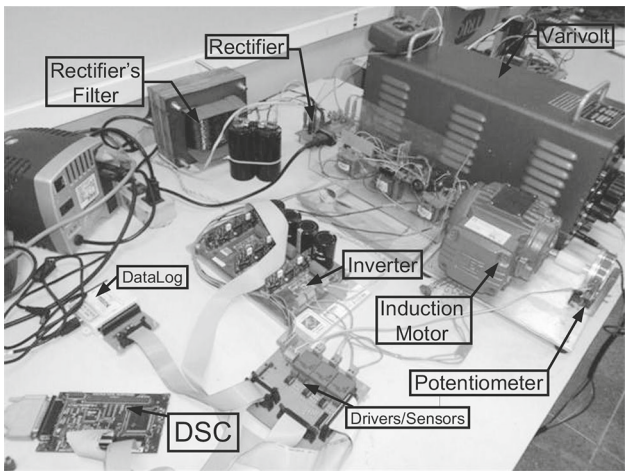

Fig. 9 Experimental setup

where $I_{\mathrm{r}}(\Omega)$ is defined as the robustness index of the controller. Figure 6 shows the robustness index $I_{\mathrm{r}}(\Omega)$ to the controller for several values of σ, considering a error of 20 % in the gain and three sample delays. From Fig. 5, in low frequencies, the robustness index for all evaluated values of s is virtually the same and in the middle frequencies the robustness index can be easily tuned by σ.

5 Simulation and experimental results

The structure proposed has been seen in Fig. 6. For implement the GPC controller was used the user-specified parameters included in the proposed method that are $N_2 = 30$, $N_{\mathrm{u}} = 1$ and $\alpha = 0.95$. The filter polynomial used $C(q^{-1}) = 1 - 1.9q^{-1} + 0.9025q^{-2}$ which corresponds to a $\sigma = 0.05$.

Using (29) to (31) the parameters RST found were: $s_0 = -0.605$, $s_1 = 0.5816$, $s_2 = 0.013$, $r_1 = -1.848$, $r_2 = 0.851$, $t_0 = -4.111$, $t_1 = 7.811$, $t_2 = -3.71$.

The proposed system was simulated considering the analysis of the following parameters: rotor position, rotor speed, direct-axis current (responsible for the field generation in the machine), and quadrature axis current (responsible for the electrical torque of the machine). Based on such data, the behavior of the rotor position reference is analyzed, corresponding to the 1 radian and after a perturbation to the

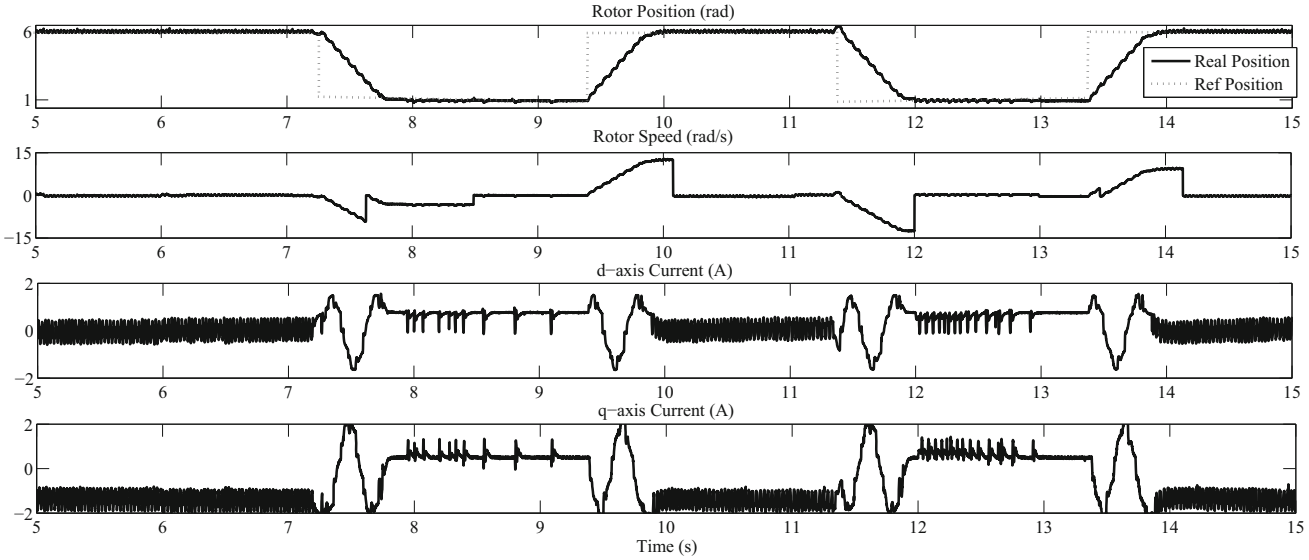

Fig. 10 Experimental results for the system using the GPC control strategy

0.2 during 2.5 s, in Fig. 7. Thus, it is possible to verify the capability of the perturbation rejection of the positioning rotor.

For the experimental implementation of the system, a kit consisting of a DSC from Texas Instruments TMS320F2812 was used. The machine is a fractional horsepower three-phase squirrel cage IM, whose parameters are given in Table 1.

The remaining instruments are Hall-effect current sensors, the auxiliary voltage sources, a three-phase voltage inverter module by Semikron with a switching frequency of 2.5 kHz, a multi-turn precision potentiometer coupled to the motor shaft, with a sampling time of 0.4 ms and for the controller was used a sampling time of 10 ms for being a slow loop. The schematics and experimental setup are shown in Figs. 8 and 9, respectively.

The same control techniques considered in the simulation tests are studied. The conditions for the reference position steps are from 6 to 1 radian after from 1 radian to 6 radians again, each step change occurs after few seconds. Thus, it is possible to verify the capability of accuracy and repeatability of the positioning rotor.

Figure 10 shows the evaluation of the GPC control strategies proposed. By observing the tracking position is about 0.5 seconds. Analyzing the behavior of the rotor speed there is a small oscillation after reaches reference and during changes reference are about 12 and −12 rad/s. The currents id in the reference changes has peaks about 1.8 A and steady state oscillation with peaks about 0.6 A. And the iq oscillates with peaks of −1.5 A in steady state and peaks about 2 A in reference changes.

An assembly was performed to verify the rejection of system disturbances implemented. Being this assembly consisting of a DC motor model manufacturer PHYWE 11610.00,

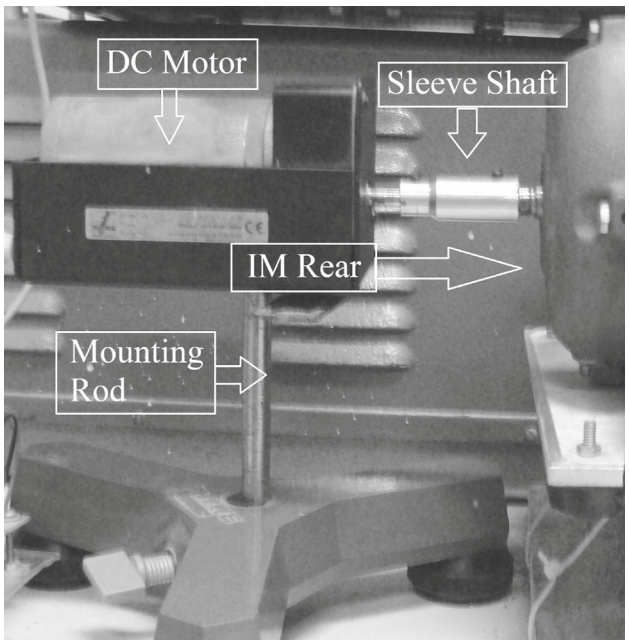

Fig. 11 Mounting for load test

which has a torque of approximately, 0.2 N m. The DC motor engine, which emulates the charge to disturbing the system, is connected to the rear axle of the IM through a shaft sleeve and is positioned by a mounting bracket for the correct alignment of engines for no slips axes when the drive DC motor, as shown in Fig. 11.

Then, carrying out the same procedure of the simulation, that is, by adding a load of 0.2 N at a given instant 18 s of the test, tests were made to examine the behavior of the controller under study.

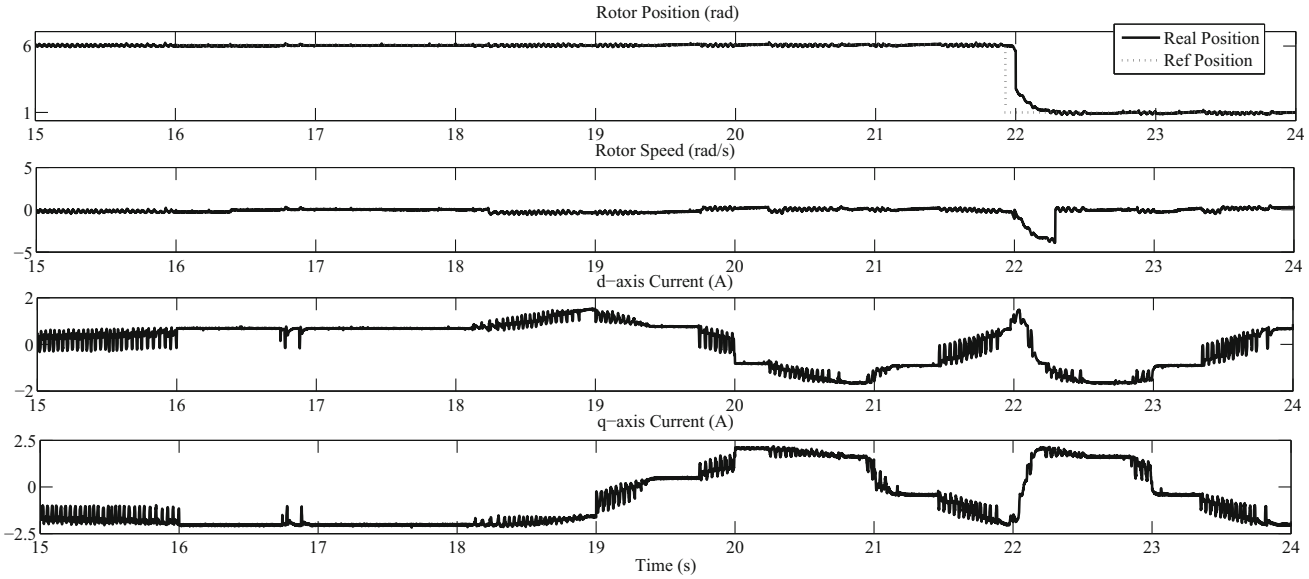

Fig. 12 Behavior GPC controller to disturbance during the experimental test

The behavior of the controller can be seen in Fig. 12. It is observed that the rotor speed has a small oscillation in perturbation instant and has a value of −4.1 rad/s in steady state. The current id and before the perturbation was about 0.62 A and after has peaks about 1.98 A and i_q have peaks of about 2.43 A and before perturbation was −2.4 A.

6 Conclusions

Controlling the position of an induction machine is particularly difficult due to existing inertia moments and low-viscous friction coefficient, which brings complexity to the control of rotor position. To analyze the performance of the controllers, the stator currents can be measured, thus representing the control system effort. The GPC strategy was then used in the studied plant providing the expected results, with good response to the reference and low swings in steady state, besides presenting a good performance of the disturbance rejection. The use of a linear model simplifies the model structure and consequently the controller to be used. The purpose of this study is to use a relatively simple controller with the strength characteristics of the predictive strategy. In a previous work [22] can be seen the use of classical models, where were shown that with the use of PID is achieved a longer time tracking position and a greater oscillation around the reference, as well as lower values of peak to i_d and i_q. Finally, such techniques can be applied to a robotic arm, while the actuation regarding of other motor and controller types is supposed to be investigated.

References

1. Bose BK (2001) AC machines for drives in modern power electronics and AC drives. Prentice Hall PTR, Englewood Cliffs
2. de Santana ES, Bim E, do Amaral WC (2008) A predictive algorithm for controlling speed and rotor flux of induction motor. IEEE Trans Ind Electron 55(12):4398–4407
3. Beerten J, Verveckken J, Driesen J (2010) Predictive direct torque control for flux and torque ripple reduction. IEEE Trans Ind Electron 57(1):404–412
4. Jacobina CB, Ribeiro LAS, Filho JBM, Salvadori F, Lima AMN (2003) Sistema de acionamento com motor de indução orientado indiretamente pelo campo com adaptação MRAC da velocidade. Rev Control Autom 14(1):41–49
5. Arab Markadeh GR, Soltani J (2006) Robust direct torque and flux control of adjustable speed sensorless induction machine drive based on space vector modulation using a PI predictive controller. Electr Eng 88(6):485–496
6. Ho T-J, Yeh L-Y (2010) Design of a hybrid PID plus fuzzy controller for speed control of induction motors. In: IEEE conference on industrial electronics and applications, pp 1352–1357
7. Halbaoui K, Boukhetala D, Boudjema F (2008) A new robust model reference adaptative control for induction motor drives using a hybrid controller. In: IEEE international symposium on power eletronics, electrical drives, automation and motion, pp 1109–1113
8. Raute R, Caruana C, Staines CS, Cilia J, Sumner M, Asher GM (2010) Sensorless control of induction machines at low and zero speed by using PWM harmonics for Rotor-Bar slotting detection. In: IEEE international conference on transations electronics, vol 46, issue 5, pp 1989–1998
9. Ying-Yu T (1996) DSP-based robust control of an AC induction servo drive for motion control. IEEE Trans Control Syst Technol 4(6):614–626
10. Egiguren PA, Oscar BC (2010) Robust position control of induction motor drives. In: IEEE international symposium on industrial electronics, pp 1468–1473
11. Chung-Yuen W, Sei-Chan K, Bose BK (1992) Robust position control of induction motor using fuzzy logic control. In: IEEE/IAS annual meeting conference record, vol 1, pp 472–481

12. Bayindir MI, Can H, Akpolat ZH, Ozdemir M, Akin E (2005) Application of reaching law approach to the position control of a vector controlled induction motor drive. Electr Eng 87(4):207–215
13. Honório DA, Diniz EC, de Souza AB, Almeida OM, Barreto LHSC (2010) Comparison between sliding model and vector control for a DSP-based position control applied to squirrel-cage induction motor. In: IEEE/IAS international conference on industry applications, pp 1–6
14. Ljung L (1999) System identification—theory for the user, 2nd edn. PTR Prentice Hall, Upper Saddle River
15. Clarke DW, Mothadi C, Tuffs PS (1987) Generalized predictive control. Part I the basic algorithm and part II extensions and interpretations. Automatica 23(2):137–160
16. Camacho EF, Bordons C (2004) Model predictive control. Springer, London
17. Torrico BC, Roca L, Normey-Rico JE, Guzman JL, Yebra L (2010) Robust nonlinear predictive control applied to a solar collector field in a solar desalination plant. IEEE Trans Control Syst Technol 18(6):1430–1439
18. De Keyser R (2003) Model based predictive control. Invited chapter in UNESCO Encyclopedia of Life Support Systems (EoLSS), article 6.43.16.1, p. 30. ISBN: 0 9542 989 18-26-34
19. Yoon TW, Clarke DW (1994) Advances in model-based predictive control, towards robust adaptive predictive control. Oxford University Press, New York, pp 402–414
20. Larsson P, Hägglund T (2011) Control signal constraints and filter order selection for PI and PID controllers. In: Proceedings of the American Control Conference 2011, San Francisco, CA, USA, pp 4994–4999
21. Skogestad S, Postlethwaite I (1996) Multivariable feedback control: analysis and design. Wiley, New York
22. de Souza AB, Diniz EC, Honório DA, Barreto LHSC, dos Reis LLN (2013) Hybrid position control technique of induction motor drive. Control Cybern 42(4):117